Theoretical and Applied Fracture Mechanics 5 (1986) 181–188
North-Holland

INTERNALLY INDENTED PENNY-SHAPED CRACKS: A COMPARISON OF ANALYTICAL AND BOUNDARY INTEGRAL EQUATION ESTIMATES

C.L. TAN and A.P.S. SELVADURAI

Faculty of Engineering, Carleton University, Ottawa, Ontario, Canada K1S 5B6

The problem of the axisymmetric internal indentation of a penny-shaped crack by a rigid circular inclusion is discussed. The paper presents a comparison of analytical and boundary integral equation results for the stress intensity factor at the boundary of the penny-shaped crack indented by a smooth inclusion. Numerical results presented in the paper examines the influence of features such as adhesion at the inclusion-elastic medium interface and finite geometry of the elastic solid containing the penny shaped crack.

1. Introduction

The stress analysis of a penny-shaped crack which is situated in an elastic solid is a classical problem in the mathematical theory of three-dimensional elastostatics. This particular problem is also of fundamental interest to the study of initiation and propagation of fracture in brittle elastic solids. The classical studies pertaining to penny-shaped cracks located in elastic media are due to Sneddon [1,2] and Sack [3]. Complete accounts of further developments in the stress analysis of penny-shaped cracks located in isotropic and transversely isotropic elastic media are given by Sneddon and Lowengrub [4], Kassir and Sih [5] and Cherepanov [6]. These reviews contain comprehensive accounts of problems wherein the penny-shaped crack is subjected to arbitrary surface tractions.

The category of problems in which the surfaces of the penny shaped crack are subjected to displacement-dependent traction boundary conditions have been investigated by Selvadurai [7,8] in connection with the mathematical analysis of flaw bridging in unidirectional fibre reinforced composites. Recently Selvadurai and Singh [9] examined the problem where a penny-shaped crack located in an isotropic elastic solid is subjected to internal indentation by a smooth penny-shaped rigid inclusion of finite thickness (Fig. 1).

The problem of internal indentation of penny-shaped cracks by inclusions is of interest to the study of thermally induced degradation of multi-phase composites. In this situation, any mismatch in the thermal expansion coefficients between a reinforcing inclusion and the matrix can initiate the penny-shaped crack (Fig. 2).

The brittle fracture propagation and stability of the created crack will be governed by the stress intensity factor at the boundary of the crack. In general, the interactions that take place at an indented penny-shaped crack are quite complex. Firstly, the geometry of the created crack may not correspond to the idealized penny-shape. Secondly, the interface between the created flaw and the indenting disc inclusion can exhibit a variety of conditions ranging from complete adhesion to complete frictionless behaviour with Coulomb

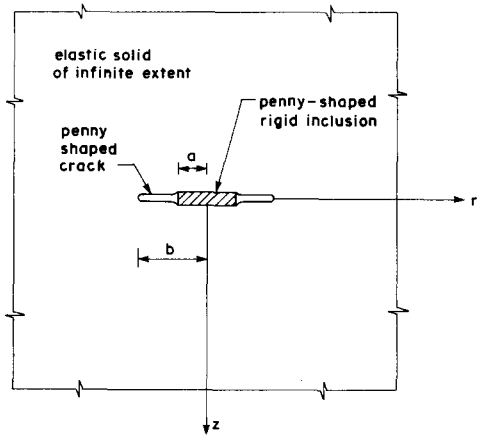

Fig. 1. Geometry of the internally indented penny-shaped crack.

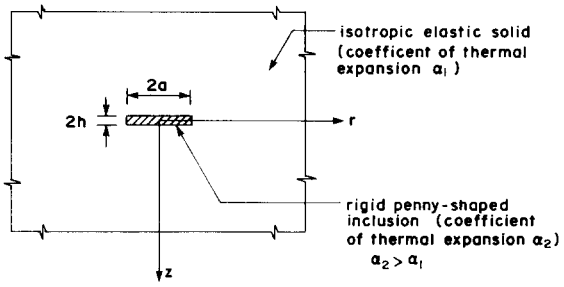

(a) Intact elastic solid containing a penny-shaped inclusion

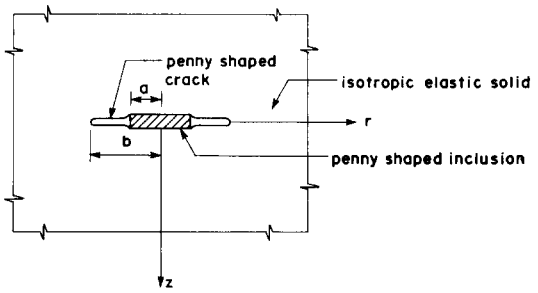

(b) Thermally induced crack

Fig. 2. A mechanism for the internal indentation of a penny-shaped crack.

friction or finite friction occupying an intermediate position.

The analytical solution of these problems is extremely complicated. For example, in the case of complete adhesion at the inclusion-crack interface, the mathematical analysis of the mixed boundary value problem gives four simultaneous singular integral equations which can be solved only in approximate fashion. In the case of frictional behaviour at the interface the solution to the internal indentation problem can be obtained only via an incremental analysis of the mixed boundary value problem. Even for the simplest form of frictionless indentation of the penny-shaped crack, the solution of the problem can be obtained only in an approximate series form; the parameter in the series expansion corresponds to the ratio of the radius of the penny-shaped rigid inclusion to the radius of the penny-shaped crack.

Numerical methods of stress analysis offer alternative techniques for examining this class of internal indentation problems related to a penny-shaped crack. Both finite element methods and boundary integral equation (BIE) techniques have been applied quite successfully for the stress analysis of crack problems (see e.g. Hilton and Sih [10], Luxmoore and Owen [11–13]). In this paper we apply the BIE method to examine the problem of the internal indentation of a penny-shaped crack located in an elastic solid. The BIE analysis of the problem takes into account a number of important features such as finite geometry of the elastic solid and adhesion at the inclusion-elastic medium interface. Numerical results presented in the paper illustrate the manner in which the stress intensity factor at the boundary of the penny-shaped crack is influenced by these extra constraints.

2. Analytical results

For completeness we shall present a very brief account of the analytical solution of the problem of the frictionless indentation of a penny-shaped crack by a rigid disc inclusion. We consider the axisymmetric problem related to an isotropic elastic infinite space which is bounded internally by a penny-shaped crack of radius b. The traction-free plane surfaces of the crack are indented by a smooth rigid circular inclusion of radius a and thickness $2h$. The indentation process is assumed to be such that complete contact is maintained between the elastic solid and the plane faces of the rigid circular disc (Fig. 1). Since the problem exhibits a state of symmetry about the plane $z = 0$, attention can be restricted to a single halfspace region of the elastic solid ($z \geqslant 0$). The mixed boundary conditions associated with the reduced halfspace problem are

$$\sigma_{rz}(r, 0) = 0, \quad 0 \leqslant r < \infty, \tag{1}$$

$$u_z(r, 0) = h, \quad 0 \leqslant r \leqslant a, \tag{2}$$

$$\sigma_{zz}(r, 0) = 0, \quad a < r < b, \tag{3}$$

$$u_z(r, 0) = 0, \quad b < r < \infty. \tag{4}$$

In addition to the mixed boundary conditions (1)–(4) the displacement and stress fields should satisfy some regularity conditions. Since the loading of the crack is such that the loads are self equilibrating, the displacement and stress fields should reduce to zero as $(r^2 + z^2)^{1/2} \to \infty$.

The axisymmetric mixed boundary value problem posed by (1)–(4) can be analysed by making

use of Love's strain potential approach (see e.g. Fung [14]). The details of the formulation are given in [9]. Briefly, a Hankel transform development of the strain potential can be employed to reduce (1)–(4) to the following system of triple integral equations for an unknown function $A(\xi)$, i.e.,

$$\int_0^\infty \xi^2 A(\xi) J_0(\xi r)\, \mathrm{d}\xi = -\frac{Gh}{(1-\nu)}, \quad 0 \leqslant r \leqslant a, \tag{5}$$

$$\int_0^\infty \xi^3 A(\xi) J_0(\xi r)\, \mathrm{d}\xi = 0, \quad a < r < b, \tag{6}$$

$$\int_0^\infty \xi^2 A(\xi) J_0(\xi r)\, \mathrm{d}\xi = 0, \quad b \leqslant r < \infty. \tag{7}$$

The triple integral equation system (5)–(7) can be solved by employing the techniques outlined by Cooke [15]. The details of this treatment are given in [9]. Briefly, it is assumed that (6) admits a representation of the form

$$\int_0^\infty \xi^3 A(\xi) J_0(\xi r)\, \mathrm{d}\xi = \begin{cases} f_1(r), & 0 < r < a, \quad (8) \\ f_2(r), & b < r < \infty. \quad (9) \end{cases}$$

Using (8) and (9), the remaining eqs. (5) and (6) can be reduced to a system of coupled integral equations of the form

$$f_1(\eta) = \frac{2}{\pi(a^2-\eta^2)^{1/2}} \times \left\{ -\frac{hG}{(1-\nu)} - \int_b^\infty \frac{t(t^2-a^2)^{1/2} f_2(t)}{(t^2-\eta^2)}\, \mathrm{d}t \right\}, \quad 0 \leqslant \eta \leqslant a, \tag{10}$$

$$f_2(\eta) = \frac{2}{\pi(\eta^2-b^2)^{1/2}} \left\{ \int_0^a \frac{t(b^2-t^2)^{1/2} f_1(t)}{(\eta^2-t^2)}\, \mathrm{d}t \right\}, \quad b \leqslant \eta < \infty. \tag{11}$$

These coupled integral equations can be further reduced to a single Fredholm integral equation of the second kind which is solved in an approximate fashion. In particular, the solution of $f_1(r)$ and $f_2(r)$ are evaluated in power series in terms of a small non-dimensional parameter. A number of such parameters can be chosen; here we select the small parameter a/b $(= c < 1)$. The results of interest to the ensuing section concerns the stress distributions at the inclusion-elastic medium interface, the stress distribution in the region $r > b$ and the stress intensity factor at the penny shaped crack boundary.

The contact stress at the inclusion-elastic medium interface is given by

$$\sigma_{zz}(r, 0) = \sigma_0 S_a(\rho, c), \quad 0 < r < a, \tag{12}$$

where

$$\sigma_0 = \frac{hG}{2(1-\nu)a}\left(1 + \frac{c}{\pi}\right),$$

$$S_a = \frac{4}{(\pi + c)(1-\rho^2)^{1/2}} \times \left\{ 1 + \frac{4}{\pi^2}c + \frac{16}{\pi^4}c^2 + c^3\left(\frac{8}{3\pi^2}\rho^2 - \frac{8}{9\pi^2} + \frac{64}{\pi^6}\right) + c^4\left(\frac{32}{3\pi^4}\rho^2 + \frac{256}{\pi^8}\right) + c^5\left[\frac{32}{15\pi^2}\rho^4 + \left(\frac{128}{3\pi^6} - \frac{8}{15\pi^2}\right)\rho^2 + \frac{1024}{\pi^{10}} + \frac{128}{9\pi^6} - \frac{28}{75\pi^2}\right] + O(c^6) \right\}. \tag{13}$$

Also, in the intact region beyond the penny-shaped flaw

$$\sigma_{zz}(r, 0) = \sigma_0 S_b(\gamma, c), \quad b < r < \infty, \tag{14}$$

where

$$S_b = \frac{2c}{(\pi + c)(\gamma^2 - 1)^{1/2}} \times \left\{ \frac{4}{\pi}\frac{c}{\gamma^2} + \frac{16}{\pi^3}\frac{c^2}{\gamma^2} + c^3\left[\frac{64}{\pi^5\gamma^2} + \frac{4(2-\gamma^2)}{3\pi\gamma^4}\right] + c^4\left[\frac{16}{\pi\gamma^2}\frac{2}{9\pi^2} + \frac{16}{\pi^6} + \frac{2-\gamma^2}{3\pi^2\gamma^2}\right] + c^5\left[\frac{4}{\pi\gamma^2} + \frac{256}{\pi^8} + \frac{16(2-\gamma^2)}{3\pi^4\gamma^2} + \frac{8-4\gamma^2-\gamma^4}{15\gamma^6}\right] + O(c^6) \right\} \tag{15}$$

and $\gamma = r/b$.

The stress intensity factor K_I at the boundary of the penny-shaped crack can be expressed in the form

$$K_I = K_0 F(c), \tag{16}$$

where

$$K_0 = \frac{hG}{\pi(1-\nu)\sqrt{b}}, \tag{17}$$

$$F(c) = \frac{4}{\pi}c + \frac{16}{\pi^3}c^2 + c^3\left(\frac{64}{\pi^5} + \frac{4}{3\pi}\right) + c^4\left(\frac{80}{9\pi^3} + \frac{256}{\pi^7}\right) + c^5\left(\frac{448}{9\pi^5} + \frac{1024}{\pi^9} + \frac{4}{5\pi}\right) + O(c^6). \tag{18}$$

It may be noted that the above procedures can be readily extended to cover the case of transversely isotropic elastic materials. In the particular instance when the axis of elastic symmetry coincides with the z-direction the stress intensity factor appropriate for the internal indentation of a penny-shaped crack located in a transversely isotropic elastic solid takes the form

$$K_I^T = K_0^T F(c), \tag{19}$$

where

$$K_0^T = \frac{h}{\pi\sqrt{b}}\left\{\frac{\sqrt{\nu_2}\,C_1(1+k_2) - \sqrt{\nu_1}\,C_2(1+k_1)}{\sqrt{\nu_1\nu_2}\,(k_1-k_2)}\right\} \tag{20}$$

with

$$C_1 = k_1 c_{33} - \nu_1 c_{13} \quad \text{and} \quad C_2 = k_2 c_{33} - \nu_2 c_{13},$$

where c_{11}, c_{33}, c_{13} etc. are the elastic constant of the transversely isotropic elastic solid [16],

$$k_\alpha = \frac{c_{11}\nu_\alpha - c_{44}}{c_{13} + c_{44}} \quad (\alpha = 1, 2), \tag{21a}$$

and ν_1 and ν_2 are the roots of the equation

$$c_{11}c_{44}\nu^2 + \{c_{13}(2c_{44} + c_{13}) - c_{11}c_{33}\}\nu + c_{33}c_{44} = 0. \tag{21b}$$

3. Review of the BIE method for axisymmetric stress analysis

The formulation of the BIE method for axisymmetric stress analysis is well documented in the literature (see e.g. [17–21]), thus only a review of the basic equations is presented here.

Consider a radial plane of an axisymmetric elastic solid, assumed isotropic and subjected to axisymmetric loads. Let S be the boundary of the radial plane that generates the axisymmetric body on rotation around the vertical axis, z. If p is a point at the interior of this plane with coordinates (R, Z) and Q is a field point on S with coordinates (r, z), then the radial displacement $u_r(p)$ and the axial displacement $u_z(p)$,at p are given, in matrix form, by Somigliana's identity as follows:

$$\begin{bmatrix} u_r(p) \\ u_z(p) \end{bmatrix} = 2\pi\int_S \begin{bmatrix} U_{rr}(p,Q) & U_{rz}(p,Q) \\ U_{zr}(p,Q) & U_{zz}(p,Q) \end{bmatrix}\begin{bmatrix} t_r(Q) \\ t_z(Q) \end{bmatrix} r \times dS(Q) - 2\pi\int_S \begin{bmatrix} T_{rr}(p,Q) & T_{rz}(p,Q) \\ T_{zr}(p,Q) & T_{zz}(p,Q) \end{bmatrix}\begin{bmatrix} u_r(Q) \\ u_z(Q) \end{bmatrix} r \times dS(Q). \tag{22}$$

In (22), the kernel functions $U_{ij}(p, Q)$ and $T_{ij}(p, Q)$ $(i, j \equiv r, z)$, denote the displacement and traction respectively in the ith direction at Q due to a unit ring load in the jth direction at p. The explicit forms of these functions are given in [18–21].

Taking $p \to P$, a boundary point on S, by the usual limiting process results in the boundary integral equations. They represent integral constraints relating the tractions and displacements at the boundary of the radial plane for a general axisymmetric problem. These equations are shown in matrix form as follows:

$$\begin{bmatrix} C_{rr}(P) & C_{rz}(P) \\ C_{zr}(P) & C_{zz}(P) \end{bmatrix}\begin{bmatrix} u_r(P) \\ u_z(P) \end{bmatrix} + 2\pi\int_S \begin{bmatrix} T_{rr}(P,Q) & T_{rz}(P,Q) \\ T_{zr}(P,Q) & T_{zz}(P,Q) \end{bmatrix}\begin{bmatrix} u_r(Q) \\ u_z(Q) \end{bmatrix} r \times dS(Q) = 2\pi\int_S \begin{bmatrix} U_{rr}(P,Q) & U_{rz}(P,Q) \\ U_{zr}(P,Q) & U_{zz}(P,Q) \end{bmatrix}\begin{bmatrix} t_r(Q) \\ t_z(Q) \end{bmatrix} r \times dS(Q), \tag{23}$$

where the values for $C_{ij}(P)$ $(i, j \equiv r, z)$ are dependent on the tangent plane(s) at P.

In order to evaluate (24), the boundary is discretized into M line segments or elements. Each of these elements is defined by three nodal points and is of the quadratic isoparametric type. The representation of geometry and the unknowns over each of these elements is in terms of quadratic shape functions of the intrinsic coordinates, $N(\xi)$, as are used in the finite element methods [22]. Thus

$$\begin{bmatrix} r(\xi) \\ z(\xi) \end{bmatrix} = \sum_{c=1}^{3} N^c(\xi) \begin{bmatrix} r^c \\ z^c \end{bmatrix}, \tag{24}$$

where r^c and z^c are the coordinates of the nodal points, and the shape functions, $N^c(\xi)$, are defined as

$$N^1(\xi) = -\tfrac{1}{2}\xi(1-\xi),$$
$$N^2(\xi) = (1-\xi^2),$$
$$N^3(\xi) = \tfrac{1}{2}\xi(1+\xi), \quad -1 \leqslant \xi \leqslant +1. \tag{25}$$

Similarly,

$$\hat{u}(\xi) \equiv \begin{bmatrix} u_r(\xi) \\ u_z(\xi) \end{bmatrix} = \sum_{c=1}^{3} N^c(\xi) \begin{bmatrix} u_r^c & r \\ u_z^c & \end{bmatrix} \tag{26}$$

and

$$\hat{t}(\xi) = \begin{bmatrix} t_r(\xi) \\ t_z(\xi) \end{bmatrix} = \sum_{c=1}^{3} N^c(\xi) \begin{bmatrix} t_r^c \\ t_z^c \end{bmatrix}. \tag{27}$$

Substitution of these parametric representations into (23) results in the following

$$[C(P^a)]\hat{u}(P^a) + 2\pi \sum_{b=1}^{M} \sum_{c=1}^{3} \hat{u}(P^{d(b,c)}) \times \int_{S_b} [T(P^a, Q)] N^c(\xi) J(\xi)\, d\xi = 2\pi \sum_{b=1}^{M} \sum_{c=1}^{3} \hat{t}(P^{d(b,c)}) \times \int_{S_b} [U(P^a, Q)] N^c(\xi) J(\xi)\, d\xi. \tag{28}$$

In (28), $[C]$, $[T]$ and $[U]$ represent the matrices shown in (23). Also, P^a is the ath node in the mesh, $d(b, c)$ is the cth node of the bth element, and $J(\xi)$ is the Jacobian of transformation. Details of the numerical integration of the kernel functions have been described elsewhere (see e.g. Bakr and Fenner [21]), hence they will not be presented here. Suffice it to say that, if there are a total of q distinct nodes, then (28) represents a system of $2q$ linear algebraic equations to be solved for the unknown modal values of tractions and displacements. The solution of these equations can be obtained by direct Gaussian elimination.

4. Numerical results

In the present study, the problem of a penny-shaped crack in an elastic cylindrical solid indented by a rigid disc-shaped inclusion, Fig. 3, was investigated using the numerical BIE method. To examine the effects of finite size of the solid on the stress intensity factor at the crack periphery, and the extent of the deviation from the analytical solution as discussed in Section 2, the following geometries were considered. Referring to Fig. 3, for $R/b = 10$, the values of H/b treated were 2.5, 5 and 10; in addition, for $H/b = 10$, the configurations with $R/b = 2.5$ and 5 were also analysed. For each of these geometries, the two ideal contact conditions between the rigid disc and the surfaces of the crack, namely, perfect smoothness and perfect adhesion, were considered for a range of $c = a/b$ between 0.1 and 0.8. In all cases, Poisson's ratio was taken as 0.3.

Figure 4 shows a typical BIE mesh idealization

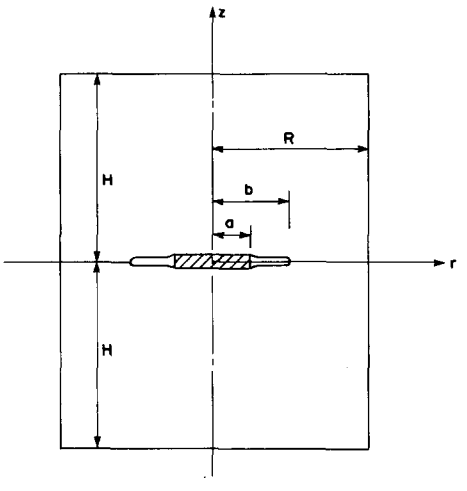

Fig. 3. Internally indented penny-shaped crack in a finite elastic solid.

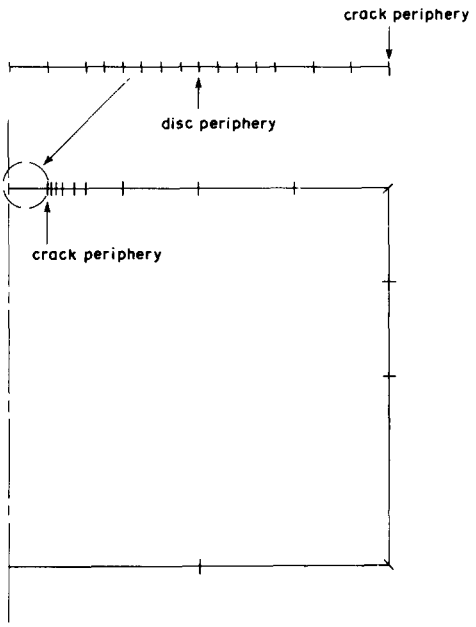

Fig. 4. BIE Mesh for $H/b = 10$, $R/b = 10$, $a/b = 0.5$.

of the physical problem. Note that only one-half of a radial plane has been modelled as advantage can be taken of the symmetry about the axial plane containing the crack. In each of the cases considered, a uniform displacement in the axial direction was applied to those elements representing the region in contact with the rigid disc. For perfect adhesion conditions, additional radial displacement constraints were imposed on these elements. Great care was taken to ensure sufficiently refined elements were used in the vicinity of the disc and crack peripheries. Indeed, it was found that the numerical results were relatively sensitive to the size of the elements there, particularly in the former area. This was to be expected as stresses are $O(1/r)$ and $O(1/\sqrt{r})$ in these regions respectively. Quarterpoint crack-tip elements were used to introduce the latter stress singularity at the crack periphery in all cases considered.

The numerical stress intensity factors, K_I, were obtained using the indirect energy method. Although this involved making two computer runs to numerically obtain the strain energy release rate and thence K_I for each cracked configuration, the cost incurred in making a second axisymmetric BIE analysis is relatively low. Besides, it has generally been established, from BIE and finite element fracture mechanics studies, that of the various schemes available for K_I computation from numerical data, the indirect energy method yields the most accurate solutions (see e.g. [23,24]).

Tables 1 and 2 show the computed values of K_I, normalized with respect to $K_0 = hG/\pi(1-\nu)\sqrt{b}$, for the cases considered. Also shown are the

Table 1
Normalized stress intensity factors K_I/K_0, $K_0 = hG/\pi(1-\nu)\sqrt{b}$, for disc indentation problem $R/b = 10$

a/b	Analytical $H/b \to \infty$ $R/b \to \infty$	H/b		
		10	5	2.5
0.1	0.133	0.136	0.139	0.155
		(0.140)	(0.143)	(0.159)
0.2	0.281	0.284	0.289	0.318
		(0.293)	(0.297)	(0.327)
0.3	0.450	0.453	0.459	0.502
		(0.468)	(0.474)	(0.516)
0.4	0.647	0.657	0.665	0.718
		(0.674)	(0.686)	(0.739)
0.5	0.882	0.900	0.911	0.972
		(0.933)	(0.942)	(1.002)
0.6	1.170	1.219	1.229	1.294
		(1.262)	(1.272)	(1.336)
0.7	1.527	1.661	1.671	1.737
		(1.722)	(1.732)	(1.797)
0.8	1.973	2.371	2.380	2.441
		(2.462)	(2.471)	(2.532)

Table 2
Normalized stress intensity factors K_I/K_0, $K_0 = hG/\pi(1-\nu)\sqrt{b}$, for disc indentation problem $H/b = 10$

a/b	Analytical $H/b \to \infty$ $R/b \to \infty$	R/b		
		10	5	2.5
0.1	0.133	0.136	0.141	0.150
		(0.140)	(0.145)	(0.154)
0.2	0.281	0.284	0.293	0.311
		(0.293)	(0.302)	(0.320)
0.3	0.450	0.453	0.466	0.492
		(0.468)	(0.481)	(0.506)
0.4	0.647	0.657	0.673	0.706
		(0.679)	(0.695)	(0.728)
0.5	0.882	0.900	0.921	0.954
		(0.933)	(0.952)	(0.990)
0.6	1.170	1.219	1.239	1.283
		(2.262)	(1.283)	(1.324)
0.7	1.527	1.661	1.708	1.723
		(1.722)	(1.772)	(1.787)
0.8	1.973	2.371	2.427	2.440
		(2.462)	(2.482)	(2.523)

analytical solutions obtained from the analysis described in Section 2 for an infinite body. The numbers in parentheses indicate the normalized K_1 values for the situation when there was a complete adhesion between the rigid disc and the crack surfaces. The results in Table 1 for the smooth contact condition are also shown in Fig. 5 for graphic comparison. It is worth noting here that computer runs had also been carried out for $R/b = H/b = 20$, $c = 0.8$, and no significant differences in the numerical results were obtained when compared with the corresponding values for $R/b = H/b = 10$. Thus the numerical solutions obtained for the latter geometry may, to all intent and purposes, be considered for an infinite body.

Considering first the smooth contact condition. It can be seen from the tables that the agreement between the analytical solution and those obtained by the BIE method for $R/b = H/b = 10$, is very good indeed for the range of c up to 0.6. As the indentation zone gets larger, the deviations between the two sets of results become more evident, increasing from about 4% for $c = 0.6$ to about 20% for $c = 0.8$. It may perhaps be worth emphasizing here again that the analytical solutions presented are not exact; the accuracies depend on the number of terms in the series expansion, in terms of c, that are used in the solution of the coupled integral equations (5)–(7), as discussed in Section 2. The values presented here are from (16) where only terms up to c^5 have been retained. In view of this, the computational results are likely to be more accurate than those predicted analytically here, especially as $c \to 1$. The results in Tables 1 and 2 also show the expected trends of increasing magnitudes of K_1 with decreasing distance between the crack and the exterior boundary. It is interesting to note that the magnifying effect on K_1 appears to be marginally greater when H/b decreases while $R/b = 10$, than when the variation of the geometry had been vice versa. Comparing the BIE results for $R/b = 10$, $H/b = 2.5$, with those predicted analytically, it can be seen that the deviations between the two sets of results, for the range of c considered, were significant, being of the order of 24%.

The BIE results also revealed that for the Poisson's ratio treated, namely 0.3, the computed stress intensity factors for the complete adhesion contact condition were only marginally higher than the corresponding values for the perfectly smooth contact condition. That the values of K_1 are relatively higher in the former situation is to be expected. Indeed, it can also be argued, on physical grounds, that for this disc indentation problem, the differences between the K_1 values for the perfectly bonded and the perfectly smooth conditions will increase as the value of the Poisson's ratio decreases.

Figure 5 shows the typical computed variation of the stress σ_{zz} in the smooth indentation region

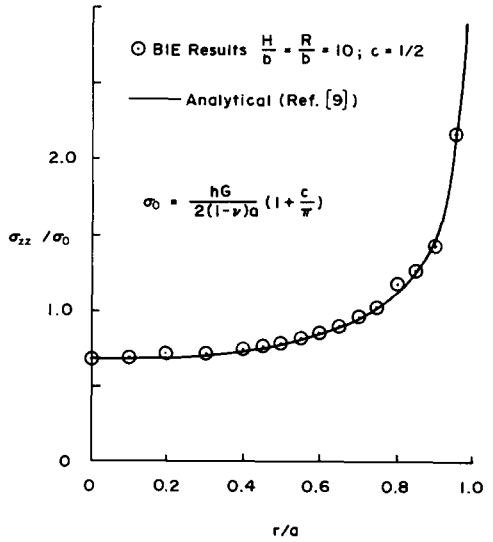

Fig. 5. The contact stress distribution $\sigma_{zz}(r, 0)$ at the inclusion-elastic medium interface.

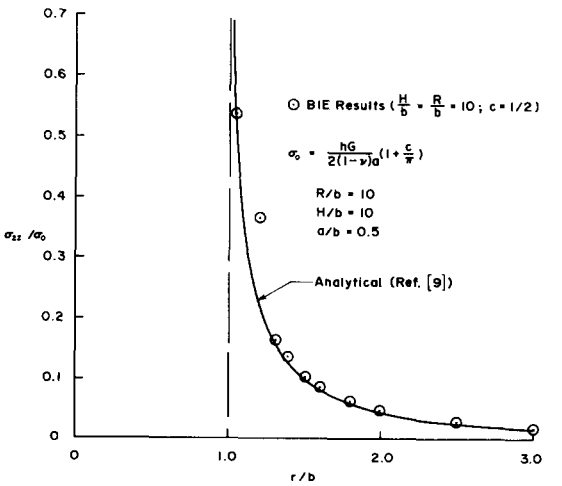

Fig. 6. The axial stress distribution $\sigma_{zz}(r, 0)$ in the region $b < r < \infty$.

of the crack surface, together with the analytical solution according to (12). As can be seen, the agreement between the two solution sets for the geometry treated, namely, $R/b = H/b = 10$, $c = 0.5$, is excellent. The computed variation of σ_{zz} ahead to the crack periphery for the same geometry and contact condition is shown in Fig. 6. Also shown plotted is the analytical prediction according to (14). Again the agreement between the computed and analytically obtained stress distributions is very good indeed, further confirming the veracity of the power series solution technique discussed in Section 2.

References

[1] I.N. Sneddon, "Stress Distribution in the Neighbourhood of a Crack in an Elastic Solid", *Proc. Royal Society*, Vol. A 187, 229–260 (1946).

[2] I.N. Sneddon, "A Note on the Problem of the Penny-shaped Crack", *Proc. Cambridge Philosophical Soc.* Vol. 61, 609–611 (1965).

[3] R.A. Sack, "Extension of Griffith's Theory of Rupture to Three Dimensions", *Phys. Soc. London*, Vo. 58, 729–736 (1946).

[4] I.N. Sneddon and M. Lowengrub, *Crack Problems in the Classical Theory of Elasticity*, Wiley, New York, (1969).

[5] M.K. Kassir and G.C. Sih, *Three Dimensional Crack Problems, Mechanics of Fracture*,Vol. 2, G.C. Sih, ed., Noordhoff, Leiden (1975).

[6] G.P. Cherepanov, *Mechanics of Brittle Fracture*, R. de Wit and W.C. Cooley, eds., McGraw-Hill, New York (1979).

[7] A.P.S. Selvadurai, "A Theoretical Model for Elastic Flaw Bridging in Uni-directional Fibre Reinforced Composites, in: A.P.S. Selvadurai, ed., *Mechanics of Structured Media, Studies in Applied Mechanics*, Vol. 5A, Elsevier Science Publ., Amsterdam, (1981) 59–72.

[8] A.P.S. Selvadurai, "Concentrated Body Force Loading of an Elastically Bridged Penny-shaped Flaw in an Unidirectional Fibre Reinforced Composite", *Internat. J. Fracture 21*, 149–159 (1983).

[9] A.P.S. Selvadurai and B.M. Singh, "On the Expansion of a Penny-shaped Crack by a Rigid Circular Disc Inclusion", *Internat. J. Fracture 25*, 69–77 (1984); *29*, R19 (1985).

[10] P.D. Hilton and G.C. Sih, "Application of the Finite Element Method to the Calculation of Stress Intensity Factors, Ch. 8, in: G.C. Sih, ed. *Methods of Analysis and Solution of Crack Problems*, Vol. 1, Noordhoff, Leiden (1973) 426–483.

[11] A.R. Luxmoore and D.R.J. Owen, eds., *Proc. First Internat. Conf. Numer. Methods in Fracture Mech.*, Swansea, (1978) 9–13.

[12] A.R. Luxmoore and D.R.J. Owen, eds., *Proc. 2nd Internat. Conf. Numer. Methods in Fracture Mech.*, Swansea, (1980) 7–11.

[13] A.R. Luxmoore and D.R.J. Owen, eds., *Proc. 3rd Internat. Conf. Numer. Methods in Fracture Mech.*, Swansea, (1984) 26–30.

[14] Y.C. Fung, *Foundations of Solid Mechanics*, Prentice Hall, New Jersey (1963).

[15] J.C. Cooke, "Triple Integral Equations", *Quart. J. Mech. Appl. Math. 16*, 193–203 (1963).

[16] A.E. Green and W. Zerna, *Theoretical Elasticity*, Clarendon Press, Oxford (1968).

[17] T. Kermanidis, "A Numerical Solution for Axially Symmetrical Elasticity", *Internat. J. Solids and Structures 11*, 493–500 (1975).

[18] M. Mayr, "On the Numerical Solution of Axisymmetric Elastic Problems Using an Integral Equation Approach", *Mech. Res. Comm. 3*, 393–398 (1976).

[19] T.A. Cruse, D.W. Snow and R.B. Wilson, "Numerical Solutions in Axisymmetric Elasticity", *Computers and Structures 7*, 445–451 (1977).

[20] F. Hartmann, Elastostatics, Ch. 4, in: C.A. Brebbia, ed., *Progress in Boundary Element Methods*, Vol. 1, Pentech Press, London (1981).

[21] A.A. Bakr and R.T. Fenner, "Boundary Integral Equation Analysis of Axisymmetric Thermoelastic Problems", *J. Strain Analysis 18*, 239–251 (1984).

[22] O.C. Zienkiewicz, *The Finite Element Method in Engineering Science*, McGraw-Hill, New York (1977).

[23] R.H. Gallagher, "A Review of Finite Element Techniques in Fracture Mechanics, in [11].

[24] C.L. Tan and R.T. Fenner, "Elastic Fracture Mechanics Analysis by the Boundary Integral Equation Method", *Proc. Royal Soc.*, Vol. A369, 243–260 (1979).